Hindawi
Journal of Nanomaterials
Volume 2022, Article ID 3720499, 9 pages
https://doi.org/10.1155/2022/3720499

Research Article

Optimization, Structural Characterization, Thermal Properties, and Bactericidal Activity of Novel Alginate/Kaolin/Ag Bionanocomposite against *Streptococcus Mutans* Biofilm

Mohammad Moslem Imani,[1] **Fatemeh Ghorbani**,[2] **Pourya Gorji**,[2] **Mohammad Salmani Mobarakeh**,[3] **and Mohsen Safaei**[3,4]

[1]*Department of Orthodontics, School of Dentistry, Kermanshah University of Medical Sciences, Kermanshah, Iran*
[2]*Students Research Committee, Kermanshah University of Medical Sciences, Kermanshah, Iran*
[3]*Advanced Dental Sciences Research Center, Kermanshah University of Medical Sciences, Kermanshah, Iran*
[4]*Division of Dental Biomaterials, School of Dentistry, Kermanshah University of Medical Sciences, Kermanshah, Iran*

Correspondence should be addressed to Mohsen Safaei; mohsen_safaei@yahoo.com

Received 26 October 2021; Revised 31 July 2022; Accepted 12 August 2022; Published 30 August 2022

Academic Editor: Lavinia Balan

Decreasing the effectiveness of existing antimicrobial agents and increasing antimicrobial resistance to them is one of the major challenges of the healthcare system. This study was aimed at determining the optimal conditions for synthesizing novel alginate/kaolin/Ag nanocomposite with the highest antimicrobial activity against *Streptococcus mutans* (*S. mutans*) biofilm. For this purpose, silver nanoparticles and alginate biopolymer were synthesized by the coprecipitation and biological methods, respectively. In situ method was used to synthesize nanocomposites. The antibacterial activity of nanocomposites against *S. mutans* biofilm was measured in 9 experiments designed by the Taguchi method to determine the highest level of antibacterial performance. Nanocomposites synthesized in experiment 3 (60 mg/ml alginate, 0.9 mg/ml kaolin, and 4 mg/ml Ag) and experiment 5 (70 mg/ml alginate, 0.6 mg/ml kaolin, and 4 mg/ml Ag) had the strongest antibacterial activity against the *S. mutans* biofilm, which completely stopped the growth of the bacterium. Various characterization tests were used to identify nanocomposite components materials that confirmed the formation of nanocomposite with desirable properties. Thermal analysis showed that the temperature range of thermal stability of nanocomposite is higher than the temperature range of thermal stability of alginate polymer. This novel nanocomposite showed desirable antibacterial potential against the *S. mutans* biofilm. As a result, it can be used as an antimicrobial and antibiofilm agent in various biomedical and dental fields.

1. Introduction

After using antibiotics in the middle of the twentieth century, the challenge of antimicrobial resistance (AMR) has steadily increased, so it seems that the continuation of this trend until 2050 could lead to 10 million more deaths each year worldwide [1]. In addition to mortality, economic problems (such as the annual cost of billions of dollars and the loss of GDP) and psychosocial-social problems (such as stigma and separation from society) can also affect different communities [2].

In the oral environment, in particular, due to biofilm formation and AMR resulting from it, we face infections that can be challenging to eradicate with conventional antimicrobial agents [3, 4]. These biofilms can also transmit AMR genes to other bacteria and thus release AMR [5]. *S. mutans* is one of the most common oral bacteria resistant to various antibiotics in oral infections [6, 7].

Introducing new antibacterial agents that can fight against bacterial agents alone or with conventional antibiotics can be an effective step in combating AMR [8]. Recently, the use of nanomaterials has attracted the

attention of researchers due to their unique properties in many fields [9–11]. The advantages of nanocomposite materials compared to conventional composites include superior thermal and mechanical properties, high surface-to-volume ratio, and high flexibility without decreasing strength, as well as desirable optical properties [12–14]. Both synthetically and naturally, polymeric nanocomposites have a high clinical application due to their availability and known properties. Alginate biopolymer has been used to produce various types of nanocomposites due to its unique properties such as low toxicity, conversion to various forms of fiber, film, and hydrogel, and biocompatibility [11, 15].

Nanoparticles have antibacterial and anticancer activities due to their shape, size, structure, and crystalline properties and have been used for disinfection [16–18]. This nanoparticle also showed good antimicrobial properties against oral pathogens such as *S. mutans*, *S. oralis*, *Lactobacillus acidophilus*, *Lactobacillus fermentum*, and *Candida albicans* and even performed better than chlorhexidine gluconate [19]. The use of silver compounds in nanocomposites can have high antimicrobial and biocompatibility properties in nanocomposites.

Kaolin is a mineral of layered phyllosilicate clay and a common compound in soils and sediments [20, 21]. Due to its cheapness, availability, and unique chemical and physical properties, this clay has been used in many health-related matters such as the food industry, wastewater treatment, and bleeding control [22–24]. Even though clay particles have no antibacterial properties, the intercalation of Ag particles on them can kill adsorbed bacteria [25]. Therefore, in the synthesis of nanocomposites, we used kaolin clay as support and adsorbent due to the challenge of the possibility of accumulating nanoparticles at the nanoscale in the polymer matrix and reducing their antibacterial performance [26].

The purpose of synthesis of this bio-nanocomposite is to use nanotechnology to fight the dental biofilm. Therefore, the present study was aimed at synthesizing and determining the optimal conditions for the antimicrobial activity of alginate/kaolin/Ag bio-nanocomposite as a novel antibacterial agent against *S. mutans* biofilm.

2. Materials and Methods

2.1. Synthesis of Alginate Biopolymer. To synthesize biopolymer alginate, *Azotobacter vinelandii* with the characteristic IBRC10786 was prepared and cultured from the Iranian biological resources center. The bacterial culture medium was then incubated for 72 h at 29°C in a shaker incubator at 150 rpm. 100 ml of the final culture medium containing the bacteria was combined with 10 ml of ethylenediaminetetraacetic acid (EDTA) (99%, Merck) 0.1 M and 10 ml of 1 M sodium chloride (99%, Merck) and centrifuged for 10 min at 5000 rpm. The supernatant was separated from the precipitated bacterial cells and stirred with isopropanol for 20 min with a magnetic stirrer. After this step, the mixture was passed through filter paper to separate the resulting sediments. The precipitate was dried in an oven at 40°C for 72 h to obtain a powdered alginate biopolymer [27].

2.2. Synthesis of Silver Nanoparticles. To synthesize silver nanoparticles, solutions containing $AgNO_3$ and trisodium citrate dihydrate ($C_6H_5Na_3O_7.2H_2O$) (99%, Merck) were prepared. 50 ml of 0.01 M silver nitrate solution was boiled, and then, 5 ml of 1% trisodium citrate was added dropwise. The resulting solution was stirred uniformly until homogeneous, and its color changed to pale yellow at 50°C. The resulting solution was centrifuged three times for 15 min using a 5000 rpm centrifuge to remove impurities [28].

2.3. Synthesis of Nanocomposites. After creating Ag nanoparticles and alginate biopolymer by the method described, kaolin clay was prepared commercially. Qulitek-4 software was used to determine the best ratio of materials for synthesizing nanocomposites with the highest antimicrobial activity, and nine experiments were designed according to the Taguchi method. For alginates, three concentrations of 60, 70, and 80 mg/ml, for silver levels of 0.3, 0.6, and 0.9 mg/ml, and for kaolin concentrations of 1, 2, and 4 mg/ml were used.

Separately, each component was stirred using distilled water solvent to disperse completely. After this step, the prepared solutions were combined using the in situ method. In this method, silver nanoparticles and kaolin solution were added simultaneously and dropwise to the alginate solution and stirred for 60 min and dispersed at room temperature for 15 min using an ultrasonic homogenizer. Finally, the resulting solution was placed in an oven for one day at a temperature of 65°C to evaporate the solvent to form nanocomposite powder sediments. After grinding in mortar as a powder, nanocomposite sediments were used to investigate its properties [29].

2.4. Antibacterial Activity. The antibacterial activity of alginate/kaolin/Ag nanocomposite against *S. mutans* biofilm was investigated. This bacterium (ATCC 35668) was prepared from the Persian type culture collection in Iran. After 24 h of culture on the brain heart infusion agar medium, single colonies of *S. mutans* were obtained. To form a bacterial biofilm, the prepared bacterial suspension equivalent to 0.5 McFarland was added to a 96-well culture plate and incubated at 37°C for 72 h. The culture medium was changed daily with fresh brain heart infusion containing 2% sucrose and 1% mannose. After biofilm formation, it was washed with PBS three times to remove planktonic. The synthesized nanocomposites were then added to the wells according to experiments designed by the Taguchi method, and the plate was incubated for 24 h at 37°C. The separated cells were then collected from the well wall to measure the number of viable cells in the biofilms. The remaining cells adhering to the well wall were suspended in 1 ml PBS buffer after three washes. The resulting suspension was then homogenized using a vortex for 2 min. To perform the colony-forming unit (CFU) test, the bacterial suspensions were diluted ten times with serial dilution, then cultured on plates containing the brain heart infusion agar, and incubated for 24 h at 37°C. After heating, the number of colonies was counted, and their mean was obtained for nine experiments. All experiments had three replications.

2.5. Characterization. The properties of alginate/kaolin/Ag nanocomposites and their components were investigated using different characterization methods. For this purpose, Fourier transform infrared spectroscopy (FTIR) (Thermo Company at RT/USA), ultraviolet-visible (UV-vis) spectrophotometry (Shimadzu Company UV-160 A model/Japan), X-ray diffraction (XRD) (Philips X 'Pert (40 kV, 30 mA)/ Netherlands), field emission scanning electron microscopy (FESEM) (TESCAN Company, MIRA III model/Czech Republic), energy dispersive X-ray spectroscopy (EDX) (MIRA III model SAMX detector/France), X-ray surface elemental mapping (Map) with SAMX detector (TESCAN Company, MIRA II model/Czech Republic), transmission electron microscope (TEM) (TEM Philips EM208S/Netherlands), and thermogravimetric analysis/differential scanning calorimetry (TGA-DSC) (TA Company, Q600 model) were used. By measuring the amount of X-ray scattering emitted for each sample, different 2θ angles at specific intensities are determined. By measuring the amount of X-ray scattering emitted for each sample, different angles 2θ at certain intensities are determined. Finally, the X-ray diffraction intensity curve is drawn in terms of angle 2θ at certain angles of the peaks corresponding to the distances between the crystal plates. From this method, the order of the crystal structure of the samples can be determined, and then, the size of the formed crystal can be determined using the Debye-Scherrer relation. In this regard, D is the crystal size, K is the crystal shape constant (0.9) close to number one, λ is the size of the X-ray cathode lamp wavelength used, B is the peak width at half the maximum height in terms of radians, and θ is diffraction angle of scattered X-ray by degree.

$$B = k\lambda/L \cos(\theta). \quad (1)$$

3. Results and Discussion

3.1. Antibacterial Activity. Nine experiments were designed to determine the optimal conditions for synthesizing alginate/kaolin/Ag nanocomposites with the highest antibacterial activity based on the Taguchi method. The effects of nanocomposites synthesized under different conditions on the viability rate of *S. mutans* were evaluated (Table 1). The results showed that the synthesized nanocomposites in experiment 3 with 60 mg/ml alginate, 0.9 mg/ml kaolin, and 4 mg/ml Ag and experiment 5 with 70 mg/ml alginate, 0.6 mg/ml kaolin, and 4 mg/ml Ag have the strongest antibacterial activity against the *S. mutans* biofilm. In their presence, the bacterial viability is reduced to zero.

Previous studies have also shown that alginate-Ag nanocomposite can have effective activity against gram-positive and gram-negative bacteria so that this effect increases with increasing concentration of silver nanoparticles and decreasing their size [30, 31]. Silver nanoparticles, due to their ability to interact with DNA and proteins containing phosphorus and sulfur, the increase of membrane permeability, and cell wall destruction, can cause the death of microorganisms, while sodium alginate biopolymer has no antibacterial properties [32]. It has also been shown that kaolin alone cannot have a good antibacterial effect; however, modifying it with Ag nanoparticles increases the antibacterial activity of nanoparticles [25].

Table 1: Taguchi design of experiments and results of antibacterial activity of alginate/kaolin/Ag nanocomposites.

Experiment	Alginate (mg/ml)			Kaolin (mg/ml)			Ag (mg/ml)			Bacterial survival (CFU/ml)
	60	70	80	0.3	0.6	0.9	1	2	4	
1		60			0.3			1		2.11
2		60			0.6			2		0.58
3		60			0.9			4		0
4		70			0.3			2		1.49
5		70			0.6			4		0
6		70			0.9			1		2.35
7		80			0.3			4		1.13
8		80			0.6			1		2.71
9		80			0.9			2		1.84

It is important to note in the toxicity of Ag nanoparticles [31]; the researchers reported that despite the high antibacterial and antibiofilm properties of Ag nanoparticles against *S. mutans* at 200 ppm, almost these nanoparticles could kill all fibroblast cells. However, due to their immobilization in the polymer matrix, the use of these nanoparticles in the form of polysaccharide nanocomposites cannot enter the eukaryotic cells and therefore lacks cytotoxicity [33, 34].

Table 2 shows the effect of alginate, kaolin, and Ag factors on the viability rate of *S. mutans* bacteria. The results showed that the alginate factor in the first level, kaolin in the second level, and Ag in the third level had the greatest effect on the viability rate of *S. mutans* bacteria.

The interaction of the factors on the viability rate of *S. mutans* bacteria is shown in Table 3. In the third level, kaolin and Ag showed the greatest interaction on the viability rate of *S. mutans* bacteria as 27/85%. Alginate in the first level and Ag in the third level had a significant interaction on the viability rate of *S. mutans* bacteria as 12/36%. The lowest interaction index was related to alginate in the first level and kaolin in the third level (0.73%).

Analysis of variance of parameters affecting the viability rate of *S. mutans* bacteria is shown in Table 4. The greatest effect on the viability rate of *S. mutans* bacteria was related to Ag with an effect of 76.29%, alginate (18.89%), and kaolin (4.29%), respectively.

After analyzing the data and examining the effect of each factor and their interaction, the optimal conditions for the synthesis of alginate/kaolin/Ag nanocomposites with the highest antibacterial activity were estimated (Table 5). Accordingly, Ag showed the highest contribution, and kaolin showed the lowest contribution on the viability rate of *S. mutans* bacteria, and alginate had an effect between these two factors and close to kaolin. The first level was the most suitable level for alginate factor, the second level for kaolin, and the third level for Ag.

Table 2: The main effects of different levels of alginate, kaolin, and Ag on the survival rate of *Streptococcus mutans*.

Factors	Level 1	Level 2	Level 3
Alginate	0.90	1.28	1.89
Kaolin	1.58	1.10	1.40
Ag	2.39	1.30	0.38

Table 3: The interactions effects of studied factors on the survival rate of *Streptococcus mutans*.

Interacting factor pairs	Column	Severity index (%)	Optimum conditions
Kaolin×Ag	2 × 3	27.85	[3, 3]
Alginate×Ag	1 × 3	12.36	[1, 3]
Alginate×kaolin	1 × 2	0.73	[1, 3]

Table 4: The analysis of variance of factors affecting the survival rate of *Streptococcus mutans*.

Factors	DOF	Sum of squares	Variance	*F*-ratio (*F*)	Pure sum	Percent (%)
Alginate	2	1.52	0.76	144.93	1.51	18.89
Kaolin	2	0.35	0.18	33.72	0.34	4.29
Ag	2	6.09	3.05	582.33	6.08	76.29

DOF: degree of freedom.

Table 5: The optimum conditions for the synthesis of alginate/kaolin/Ag nanocomposites with the highest antibacterial activity.

Factors	Level	Contribution
Alginate	1	-0.46
Kaolin	2	-0.26
Ag	3	-0.98
Total contribution from all factors		-1.70
Current grand average of performance		1.36
Bacterial survival at optimum condition		-0.34

3.2. FTIR Analysis. The results of FTIR spectroscopy showed the interaction and change of chemical composition of different components of the nanocomposite (Figure 1). In the FTIR alginate spectrum (Figure 1(a), a wide absorption band corresponding to OH at 3417 cm^{-1} and one absorption band related to CH tension at 2924 cm^{-1} were observed. The peaks at 1618 cm^{-1} and 1419 cm^{-1} were assigned to the symmetric and asymmetric tensile vibrations of carboxylate anions, respectively. The absorption band observed at 1033 cm^{-1} was attributed to the cyclic tension of COC ether [35].

In the kaolin FTIR diagram (Figure 1(b)), the peak seen at 528 cm^{-1} due to vibrations is $Al4^{+}$-O-Si, where $Al4^{+}$ is in

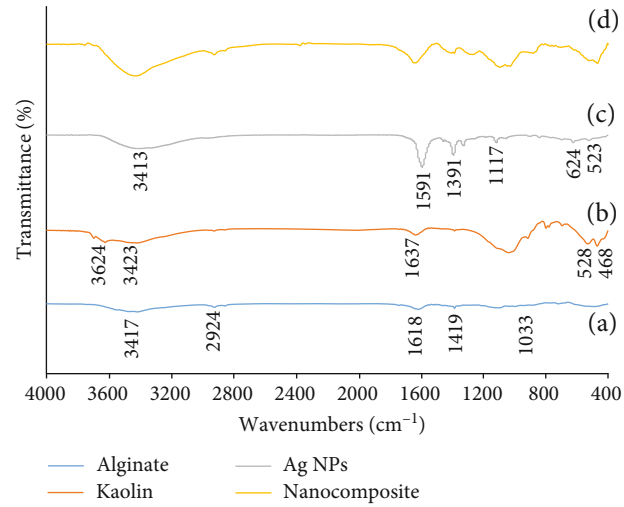

Figure 1: Infrared Fourier transform spectra of alginate (a), kaolin (b), Ag NPs (c), and alginate/kaolin/Ag nanocomposite (d).

an octagonal structure. The absorption band at 468 cm^{-1} is related to the vibration bending of the O-Si-O bond. The bands in the 3624 cm^{-1} and 3423 cm^{-1} positions are due to the tensile vibrations of the OH groups located at the edges of the kaolin plates. Also, the bands in 1637 cm^{-1} and 3624 cm^{-1} can be absorbed due to the vibration bending of the H-O-H bond of water molecules [36].

In the FTIR spectrum of silver nanoparticles (Figure 1(c)), the peaks observed in the positions of 624 cm^{-1}, 1391 cm^{-1}, and 1117 cm^{-1} are due to carbon bonds and indicate the presence of impurity compounds absorbed on the surface of Ag metal nanoparticles. Peaks were also observed at 1591 cm^{-1} due to the tensile of the C=C bond and at position 3413 cm^{-1} due to the tensile vibrations of the O-H bond [37]. The peak of 523 cm^{-1} may be due to the presence of a low amount of Ag-O nanoparticles [28].

Correlation of the component spectra with the FTIR spectrum of the synthesized alginate/kaolin/Ag nanocomposite (Figure 1(d)) showed that the final nanocomposite spectrum is composed of the resultant and overlapping spectra of its components, which confirms the optimal formation of the final nanocomposite.

3.3. UV-Vis Analysis. The ultraviolet-visible absorption spectrum of the synthesized nanocomposite and its components was recorded in the range of 200 to 800 nm (Figure 2). The alginate biopolymer spectrum (Figure 2(a)) at about 276 nm showed a wide absorption band. In the UV spectrum of kaolin clay, an absorption peak in the range of 260 nm was observed. A sharp absorption band at 208 nm and two wide absorption bands at 265 and 333 nm were observed in the UV absorption spectrum, indicating different sizes of synthesized Ag nanoparticles (Figure 2(c)). To identify the type of metal in the sample or to understand the changes in the environment around the nanomaterials, the absorption wavelength of the material can be confirmed using visible spectroscopy in visible-ultraviolet rays [28]. The lack of peak resolution in the UV absorption spectrum for the final

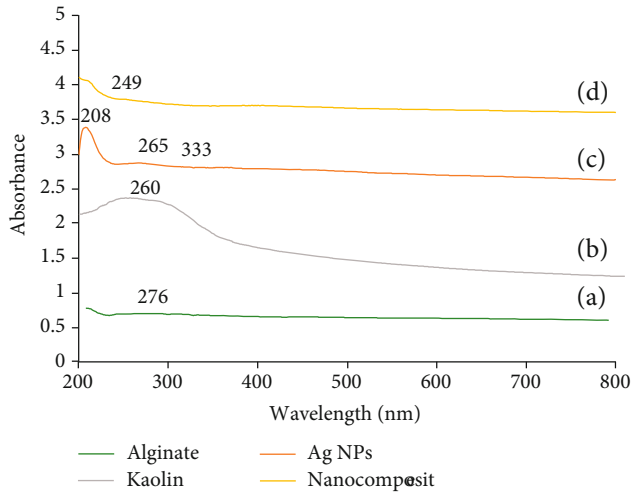

Figure 2: UV-visible of alginate (a), kaolin (b), Ag NPs (c), and alginate/kaolin/Ag nanocomposite (d).

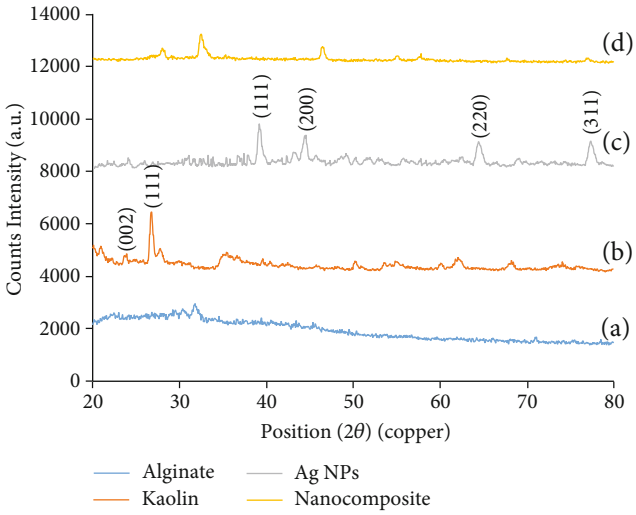

Figure 3: XRD pattern of alginate (a), kaolin (b), Ag NPs (c), and alginate/kaolin/Ag nanocomposite (d).

nanocomposite (Figure 2(d)) and the presence of a wide absorption peak in the range above 249 nm indicate the production of absorption in different sizes.

3.4. XRD Analysis. X-ray diffraction analysis of alginate biopolymer (Figure 3(a)), kaolin (Figure 3(b)), Ag nanoparticles (Figure 3(c)), and synthesized nanocomposites (Figure 3(d)) were performed to investigate the crystal behavior and fuzzy identification of nanocomposite components. The X-ray diffraction pattern of alginate biopolymer showed an amorphous structure for this material.

In the X-ray diffraction pattern of kaolin clay, the peak corresponding to the diffraction plate (002) at 23.90 indicated the presence of kaolin. Also, the 2θ angles, between 20 and 24, are related to the diffraction plates (002), (020), (101), (021), and (111). Evidence of quartz can be seen from the peak at 26.7 on the plate (111). The average crystal size for the highest peak (111) was 27 nm [38]. In the X-ray diffraction pattern of silver nanoparticles, the Miller indices of the plates (hkl), (111), (200), (220), and (311) were calculated at angles 2θ, 39.0, 44.3, 64.6, and 77.2 degrees, respectively [37]. Studying the X-ray diffraction pattern of Ag nanoparticles confirmed that the synthesized particles are silver nanoparticles with (FCC) structure [39]. The size of kaolin and silver NPs was calculated to be 27 and 21 nm using the Scherer equation.

The mean crystal X-ray diffraction pattern obtained from alginate/kaolin/Ag nanocomposite (Figure 3(d)) showed the reduction of intensity, removal of some peaks or flattening, and their movement to the left or right in the X-ray diffraction spectrum of the synthesized nanocomposite compared to the X-ray diffraction pattern of components. The main reason for this is the change in distances between the crystal plates due to the mixing of components, which showed the formation of nanocomposites.

3.5. SEM Analysis. To determine the morphology of the synthesized nanocomposite and its components, scanning electron microscope images were taken from them, which are shown in Figure 4. Figure 4(a) shows a network of alginate biopolymer acting as the matrix in the final nanocomposite. Also, the image of the microscopic structure of kaolin clay is presented in Figure 4(b). The small size of silver nanoparticles (Figure 4(c)) and their high surface to volume ratio caused the accumulation of Ag nanoparticles. Also, scanning electron microscopy images of Ag nanoparticles showed a relatively spherical shape of these nanoparticles. Scanning electron microscopy image of the final nanocomposite shows the placement of nanoparticles on the matrix (Figure 4(d)).

3.6. EDX Analysis. Energy dispersive X-ray spectroscopy (EDX) analysis of alginate/kaolin/Ag nanocomposites showed the presence of synthesized nanocomposite elements (Figure 5). These elements include silver (with 22.32% by mass, 4.92 At%), oxygen (with 34.84% by mass, 51.77 At%), aluminum (with 4.88% by mass, 4.30 At%), nitrogen (with 0.94% by mass, 1.59 At%), silicon (with 6.94% by mass, 5.88 At%), sodium (with 11.20% by mass, 11.58 At%), carbon (with 4.84% by mass, 9.57 At%), phosphorus (with 9.98% by mass, 7.66 At%), and chlorine (with 4.06% by mass, 2.72 At%).

3.7. Map Analysis. The X-ray surface elemental mapping (map) for alginate/kaolin/Ag nanocomposites is shown in Figure 6. The dispersion of oxygen, silver, sodium, phosphorus, silicon, aluminum, carbon, chlorine, and nitrogen and the dispersion in the overall composition of the synthesized nanocomposite uniformly confirmed the formation of the nanocomposite.

3.8. TEM Analysis. The transmission electron microscope (TEM) image taken from the synthesized nanocomposite showed the shape and dispersion of the nanocomposite components (Figure 7). The darker dots (nanoparticles) in the image have a higher density where the lower density material (background) is located. This shows the

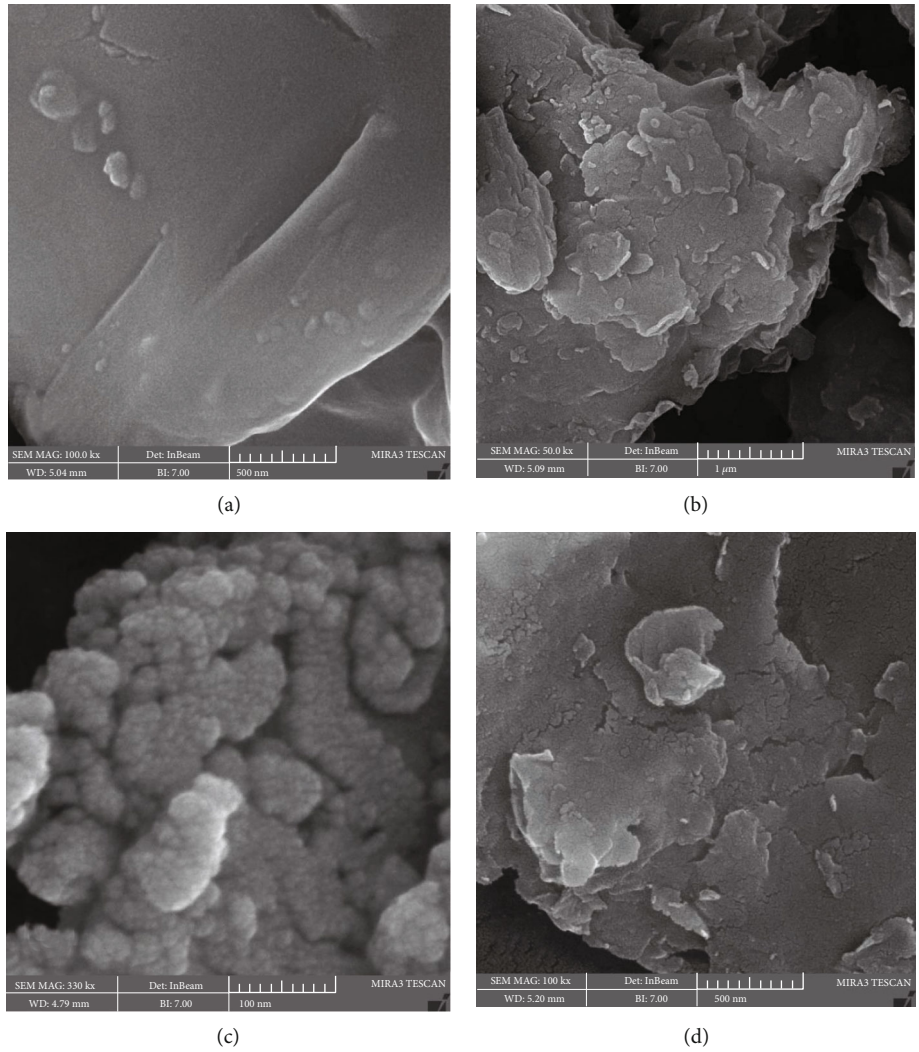

Figure 4: The scanning electron microscope image of alginate (a), kaolin (b), Ag NPs (c), and alginate/kaolin/Ag nanocomposite (d).

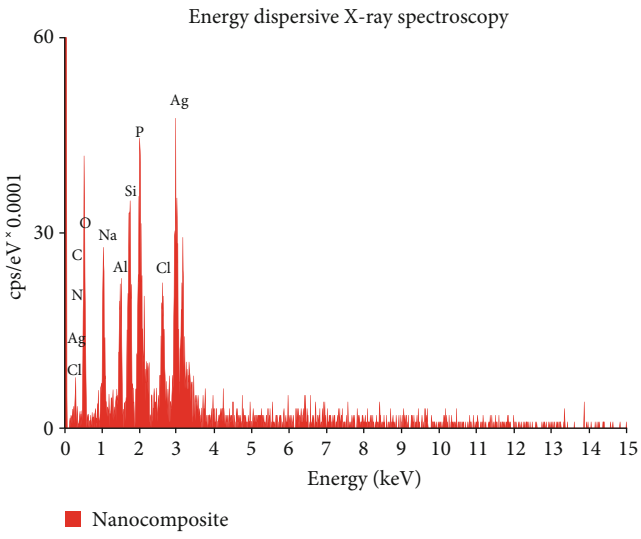

Figure 5: The energy dispersive X-ray (EDX) pattern of alginate/kaolin/Ag nanocomposite.

composition of the components and the formation of the nanocomposite.

3.9. TGA-DTA Analysis. To investigate the heat degradation behavior and thermal stability of the synthesized nanocomposite, the thermogravimetric analysis/differential scanning calorimetry analysis curve of nanocomposite and its components in the temperature range of 25 to 800°C under argon gas with a temperature increase of 20°C per min was shown in Figure 8.

Thermogravimetric analysis curve related to alginate biopolymer (Figure 8(a)) showed low thermal stability and high weight loss with increasing heat for this material. Also, the thermogravimetric analysis curve related to kaolin clay (Figure 8(b)) showed the ceramic nature, relatively high thermal stability, and slight weight loss with increasing heat.

Thermogravimetric analysis curve related to alginate/kaolin/Ag nanocomposite (Figure 8(c)) showed that the thermal stability is great by adding silver and kaolin nanoparticles to the alginate biopolymer increased. This confirms the formation of nanocomposites. In the nanocomposite

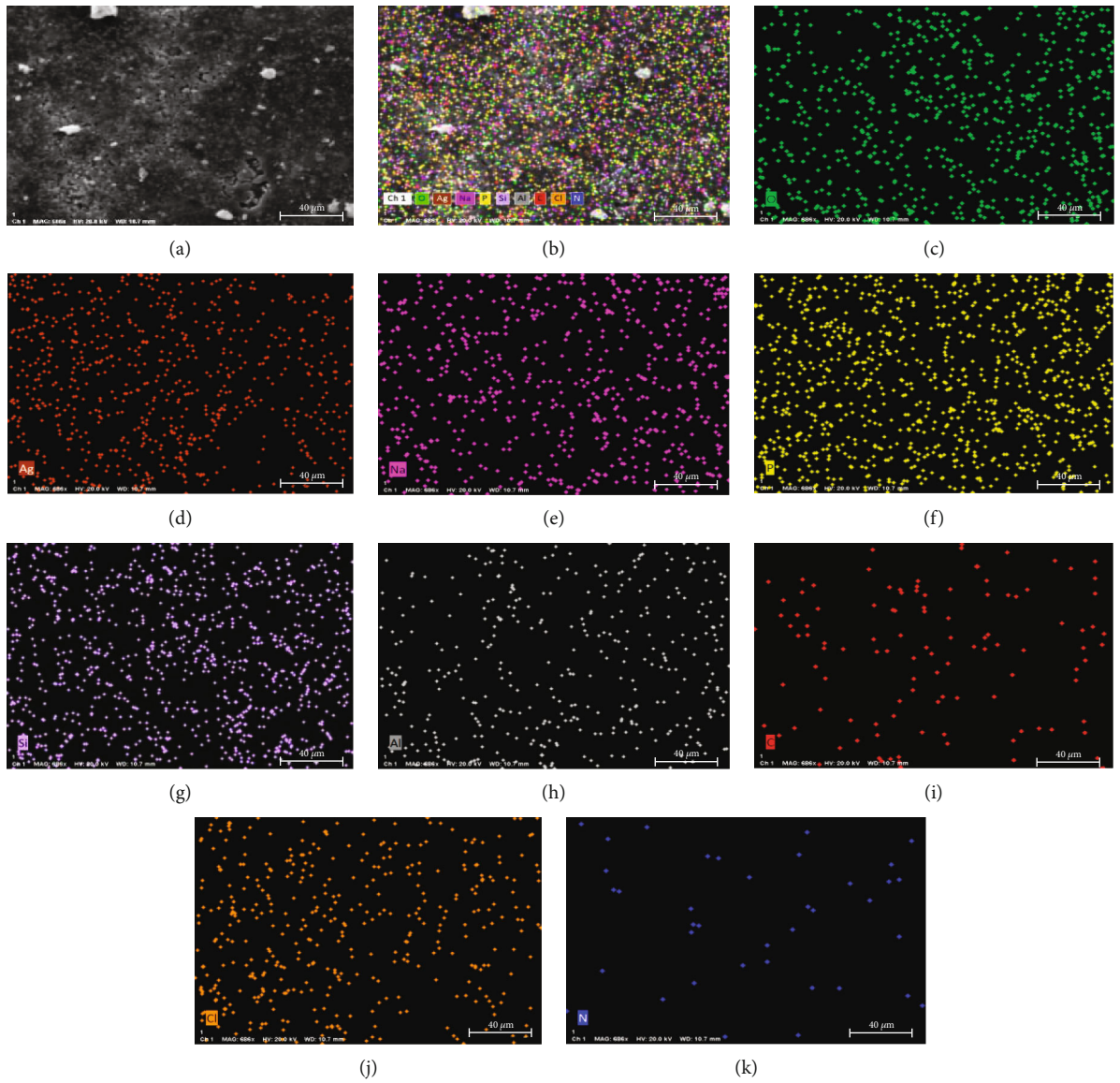

Figure 6: Dispersion map of composition components on the surface of final nanocomposite (a), all elements (b), oxygen (c), silver (d), sodium (e), phosphorus (f), silicon (g), aluminum (h), carbon (i), chlorine (j), and nitrogen (k).

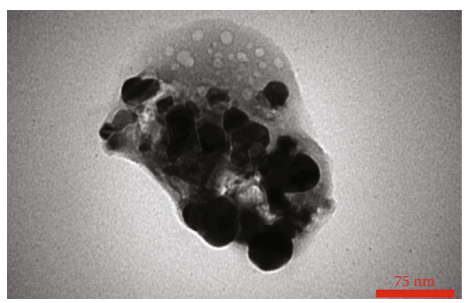

Figure 7: The transmitted electron microscope image of alginate/kaolin/Ag nanocomposite.

differential scanning calorimetry analysis diagram, upward peaks are endothermic and downward peaks are exothermic. The thermogravimetric analysis diagram and nanocomposite differential scanning calorimeter analysis curve (Figure 8(c)) showed three temperature ranges. Weight loss in the temperature range of 25 to 200°C is related to the loss of moisture and absorbed water. The amount of polymer affects the amount of water absorbed, effective in this temperature range. In the temperature range of 200 to 400°C, the polymer bonds are broken, and the polymer in the nanocomposite composition is decomposed, as shown by the appearance of peaks in the DTA diagram. In the temperature range of 400 to 800°C, structural water bonded hydroxyl groups and bonds in impurities are decomposed. Thermal decomposition of nonpolymer components is also performed in the third temperature range. Thermogravimetric analysis curves for the samples of polymer alginate, kaolin, and final nanocomposite indicated that the temperature range of thermal stability of the nanocomposite is between the temperature range of thermal stability of polymer

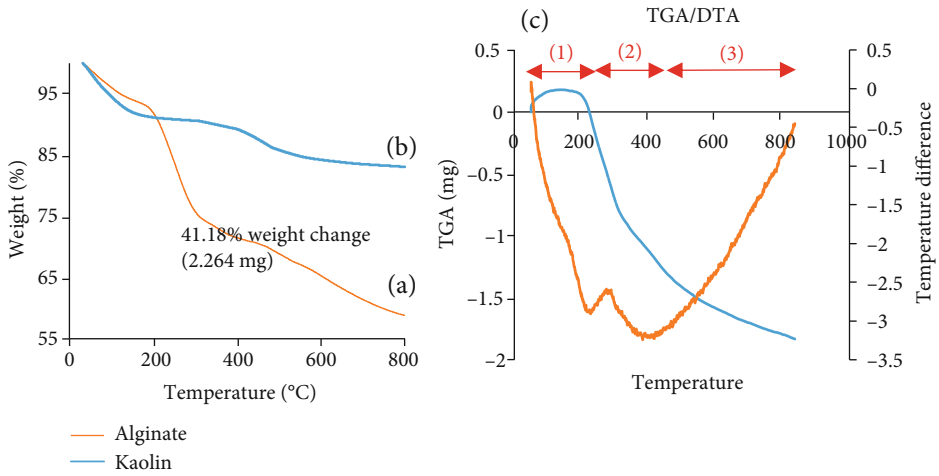

Figure 8: Thermogravimetric analysis (TGA) of alginate (a) and TGA-DTA of alginate/kaolin/Ag nanocomposite (b).

alginate and the temperature range of thermal stability of kaolin, which shows the effect of adding silver and kaolin metal nanoparticles to the polymer base and modifying the thermal stability.

4. Conclusions

The experiments showed that the new composition nanocomposite made of alginate/kaolin/Ag has a favorable antimicrobial potential against *S. mutans* biofilm, according to the results discussed. In such a way that in the right proportion of components, the growth and viability of the bacterium reach zero. These results concerning the issue of microbial resistance can be very promising, and this nanocomposite can be considered for making various preventive and therapeutic compounds.

Data Availability

No data were used to support this study.

Conflicts of Interest

The authors declare that they have no conflict of interest.

Acknowledgments

This work was supported by grants (990478) from the Kermanshah University of Medical Sciences.

References

[1] L. J. Shallcross, S. J. Howard, T. Fowler, and S. C. Davies, "Tackling the threat of antimicrobial resistance: from policy to sustainable action," *Philosophical Transactions of the Royal Society B: Biological Sciences*, vol. 370, no. 1670, article 20140082, 2015.

[2] N. R. Naylor, R. Atun, N. Zhu et al., "Estimating the burden of antimicrobial resistance: a systematic literature review," *Control*, vol. 7, no. 1, p. 58, 2018.

[3] Y. Jiao, F. R. Tay, L. N. Niu, and J. H. Chen, "Advancing antimicrobial strategies for managing oral biofilm infections," *International Journal of Oral Science*, vol. 11, no. 3, p. 28, 2019.

[4] H. Moradpoor, M. Safaei, H. R. Mozaffari et al., "An overview of recent progress in dental applications of zinc oxide nanoparticles," *RSC Advances*, vol. 11, no. 34, pp. 21189–21206, 2021.

[5] A. P. Roberts and P. Mullany, "Oral biofilms: a reservoir of transferable, bacterial, antimicrobial resistance," *Expert Review of Anti-Infective Therapy*, vol. 8, no. 12, pp. 1441–1450, 2010.

[6] B. William, C. M. Rwenyonyi, G. Swedberg, and F. Kironde, "Cotrimoxazole prophylaxis specifically selects for cotrimoxazole resistance in Streptococcus mutans and Streptococcus sobrinus with varied polymorphisms in the target genes folA and folP," *International Journal of Microbiology*, vol. 2012, Article ID 916129, 2012.

[7] M. Nilsson, T. H. Jakobsen, M. Givskov, S. Twetman, and T. Tolker-Nielsen, "Oxidative stress response plays a role in antibiotic tolerance of Streptococcus mutans biofilms," *Microbiology*, vol. 165, no. 3, pp. 334–342, 2019.

[8] M. M. D'Andrea, M. Fraziano, M. C. Thaller, and G. M. Rossolini, "The urgent need for novel antimicrobial agents and strategies to fight antibiotic resistance," *Antibiotics*, vol. 8, no. 4, p. 254, 2019.

[9] M. Safaei, M. Taran, M. M. Imani et al., "Application of Taguchi method in the optimization of synthesis of cellulose-MgO bionanocomposite as antibacterial agent," *Polish Journal of Chemical Technology*, vol. 21, no. 4, pp. 116–122, 2019.

[10] N. Hussain, S. Alwan, H. Alshamsi, and I. Sahib, "Green synthesis of S-and N-codoped carbon nanospheres and application as adsorbent of Pb (II) from aqueous solution," *International Journal of Chemical Engineering.*, vol. 2020, article 9068358, 2020.

[11] Z. H. Abdulhusain, H. A. Alshamsi, and M. Salavati-Niasari, "Facile synthesis of Au/ZnO/RGO nanohybrids using 1,8-diamino-3,6-dioxaoctan as novel functional agent for photodegradation water treatment," *Journal of Materials Research and Technology*, vol. 15, pp. 6098–6112, 2021.

[12] H. A. Alshamsi and B. S. Hussein, "Hydrothermal preparation of silver doping zinc oxide nanoparticles: study the characterization and photocatalytic activity," *Oriental Journal of Chemistry*, vol. 34, no. 4, pp. 1898–1907, 2018.

[13] S. Tharani, D. Bharathi, and R. Ranjithkumar, "Extracellular green synthesis of chitosan-silver nanoparticles using Lactobacillus reuteri for antibacterial applications," *Biocatalysis and Agricultural Biotechnology*, vol. 30, article 101838, 2020.

[14] C. N. Nandana, M. Christeena, and D. Bharathi, "Synthesis and characterization of chitosan/silver nanocomposite using rutin for antibacterial, antioxidant and photocatalytic applications," *Journal of Cluster Science*, vol. 33, no. 1, pp. 269–279, 2022.

[15] G. C. Porter, D. R. Schwass, G. R. Tompkins, S. K. Bobbala, N. J. Medlicott, and C. J. Meledandri, "AgNP/alginate nanocomposite hydrogel for antimicrobial and antibiofilm applications," *Carbohydrate Polymers*, vol. 251, article 117017, 2021.

[16] D. Bharathi, S. Vasantharaj, and V. Bhuvaneshwari, "Green synthesis of silver nanoparticles using Cordia dichotoma fruit extract and its enhanced antibacterial, anti-biofilm and photo catalytic activity," *Materials Research Express*, vol. 5, no. 5, article 055404, 2018.

[17] H. Moradpoor, M. Safaei, F. Rezaei et al., "Optimisation of cobalt oxide nanoparticles synthesis as bactericidal agents," *Journal of Medical Sciences*, vol. 7, no. 17, pp. 2757–2762, 2019.

[18] R. Razavi, M. Amiri, H. A. Alshamsi, T. Eslaminejad, and M. Salavati-Niasari, "Green synthesis of Ag nanoparticles in oil-in-water nano-emulsion and evaluation of their antibacterial and cytotoxic properties as well as molecular docking," *Arabian Journal of Chemistry*, vol. 14, no. 9, article 103323, 2021.

[19] N. P. Panpaliya, P. T. Dahake, Y. J. Kale et al., "In vitro evaluation of antimicrobial property of silver nanoparticles and chlorhexidine against five different oral pathogenic bacteria," *The Saudi Dental Journal*, vol. 31, no. 1, pp. 76–83, 2019.

[20] M. Safaeikatouli, Y. Jafariahangari, and A. Baharlouei, "Effects of dietary inclusion of sodium bentonite on biochemical characteristics of blood serum in broiler chickens," *International Journal of Agriculture and Biology*, vol. 12, no. 6, pp. 877–880, 2010.

[21] M. Safaeikatouli, F. Boldaji, B. Dastar, and S. Hassani, "The effect of dietary silicate minerals supplementation on apparent ileal digestibility of energy and protein in broiler chickens," *International Journal of Agriculture and Biology*, vol. 14, no. 2, 2012.

[22] S. Mustapha, J. Tijani, M. Ndamitso et al., "The role of kaolin and kaolin/ZnO nanoadsorbents in adsorption studies for tannery wastewater treatment," *Scientific Reports*, vol. 10, no. 1, pp. 1–22, 2020.

[23] Y. Liang, C. Xu, G. Li, T. Liu, J. F. Liang, and X. Wang, "Graphene-kaolin composite sponge for rapid and riskless hemostasis," *Colloids and Surfaces B: Biointerfaces*, vol. 169, pp. 168–175, 2018.

[24] I. N. A. Najwa, M. M. Yusoff, and Z. N. Hanani, "Potential of silver-kaolin in gelatin composite films as active food packaging materials," *Food Packaging and Shelf Life*, vol. 26, article 100564, 2020.

[25] S. K. Jou and N. A. N. N. Malek, "Characterization and antibacterial activity of chlorhexidine loaded silver-kaolinite," *Applied Clay Science*, vol. 127-128, pp. 1–9, 2016.

[26] L. Y. Ozer, A. Yusuf, J. M. Uratani et al., "Water microbial disinfection via supported nAg/kaolin in a fixed-bed reactor configuration," *Applied Clay Science*, vol. 184, article 105387, 2020.

[27] C. Peña, N. Campos, and E. Galindo, "Changes in alginate molecular mass distributions, broth viscosity and morphology of Azotobacter vinelandii cultured in shake flasks," *Applied Microbiology and Biotechnology*, vol. 48, no. 4, pp. 510–515, 1997.

[28] Y. Dasaradhudu and M. A. Srinivasan, "Synthesis and characterization of silver nano particles using co-precipitation method," *Materials Today: Proceedings*, vol. 33, pp. 720–723, 2020.

[29] M. Safaei, M. Taran, L. Jamshidy et al., "Optimum synthesis of polyhydroxybutyrate-Co_3O_4 bionanocomposite with the highest antibacterial activity against multidrug resistant bacteria," *International Journal of Biological Macromolecules*, vol. 158, pp. 477–485, 2020.

[30] B. Domènech, M. Muñoz, D. Muraviev, and J. Macanás, *Polymer-Silver Nanocomposites as Antibacterial Materials*, Microbial Pathogens and Strategies for Combating them: Science, Technology and Education, Badajoz, 2013.

[31] M. A. Pérez-Díaz, L. Boegli, G. James et al., "Silver nanoparticles with antimicrobial activities against Streptococcus mutans and their cytotoxic effect," *Materials Science and Engineering: C*, vol. 55, pp. 360–366, 2015.

[32] Y. Shao, C. Wu, T. Wu et al., "Green synthesis of sodium alginate-silver nanoparticles and their antibacterial activity," *International Journal of Biological Macromolecules*, vol. 111, pp. 1281–1292, 2018.

[33] A. Travan, C. Pelillo, I. Donati et al., "Non-cytotoxic silver nanoparticle-polysaccharide nanocomposites with antimicrobial activity," *Biomacromolecules*, vol. 10, no. 6, pp. 1429–1435, 2009.

[34] V. Ambrogi, D. Pietrella, A. Donnadio et al., "Biocompatible alginate silica supported silver nanoparticles composite films for wound dressing with antibiofilm activity," *Materials Science and Engineering: C*, vol. 112, article 110863, 2020.

[35] H. I. Chiu, A. D. Ayub, S. N. A. Mat Yusuf, N. Yahaya, E. Abd Kadir, and V. Lim, "Docetaxel-loaded disulfide cross-linked nanoparticles derived from thiolated sodium alginate for colon cancer drug delivery," *Pharmaceutics*, vol. 12, no. 1, p. 38, 2020.

[36] M. A. Tantawy and A. A. Alomari, "Extraction of alumina from Nawan kaolin by acid leaching," *Oriental Journal of Chemistry*, vol. 35, no. 3, pp. 1013–1021, 2019.

[37] K. Anandalakshmi, J. Venugobal, and V. Ramasamy, "Characterization of silver nanoparticles by green synthesis method using Pedalium murex leaf extract and their antibacterial activity," *Applied Nanoscience*, vol. 6, no. 3, pp. 399–408, 2016.

[38] G. Kesavan and S. M. Chen, "Carbon-modified kaolin clay using sugar dehydration technique for the electrochemical detection of quercetin," *Journal of Materials Science: Materials in Electronics*, vol. 31, no. 23, pp. 21670–21681, 2020.

[39] T. Theivasanthi and M. Alagar, "Electrolytic synthesis and characterization of silver nanopowder," *Nano Biomedicine and Engineering*, vol. 4, no. 2, pp. 58–65, 2012.